

# Eulerian Trilogy

Dengfeng Sun\*, Samuel D. Yang\*, Issam Strub\*, Alexandre M. Bayen<sup>†</sup>

*University of California, Berkeley, Berkeley, CA 94720-1710, USA.*

Banavar Sridhar<sup>‡</sup>, Kapil Sheth<sup>‡</sup>

*NASA Ames Research Center, Moffett Field, CA 94035, USA.*

Three Eulerian models are implemented on a graph model of air traffic flow developed in earlier work which is constructed based on one week of ASDI/ETMS data. They are applied to high altitude traffic for a full Air Route Traffic Control Center of the National Airspace System and surrounding airspace. Simulations are carried out for a full day of data to assess the predictive capabilities of the respective models. The models' predictions are compared to the real flight data (ASDI/ETMS). Several error metrics are used to characterize the relative accuracy of the models. The efficiencies of the models are compared in terms of computational time and memory requirements for the scenario of interest. An example of calibration of one of the models shows how to improve model performance. A discussion of the three models' structural differences explains why one model may outperform another.

## Nomenclature

*Sector number and corresponding sector name:*

- 1 Sector ZOA13
- 2 Sector ZOA14
- 3 Sector ZOA15
- 4 Sector ZOA31
- 5 Sector ZOA32
- 6 Sector ZOA33
- 7 Sector ZOA34
- 8 Sector ZOA35
- 9 Sector ZOA36
- 10 Sector ZOA43

## I. Introduction

The almost uninterrupted growth of US air traffic over the last few decades has motivated the design of a semi-automated *Air Traffic Control* (ATC) system to help Air Traffic Controllers manage the increasing complexity of traffic flow in the en route airspace.<sup>1</sup> ATC is operated at the sector level, where a sector is a small portion of the airspace controlled by a single human Air Traffic Controller. *Traffic Flow Management* (TFM) typically deals with traffic at the *Center* level, i.e. 10 to 20 sectors. TFM problems include maintaining the aircraft count in each sector below a legal threshold in order to ease the human ATC workload, as well as to ensure the safety of the flights.<sup>2</sup> This task is quite cumbersome; furthermore, extensive traffic forecast simulations (including all airborne aircraft) are computationally too expensive to include systematic investigations of traffic patterns that lead to sector overload. As a result, a new class of traffic flow models has emerged from recent studies: *Eulerian* models, which are control volume based. This is in contrast to

---

\*Ph.D. Students, Department of Civil and Environmental Engineering.

<sup>†</sup>Assistant Professor, Department of Civil and Environmental Engineering.

<sup>‡</sup>NASA Ames Research Center, Moffett Field, CA 94035, USA.

*Lagrangian* models, which are trajectory-based and take into account all aircraft trajectories. Unlike Lagrangian models which focus on the history of a given material element therefore using the position vector of the material element and time as variables, the Eulerian models provides a picture of the spatial distribution of the flow in function of position in space and time.

Eulerian models have two main advantages over Lagrangian models. (i) They are computationally tractable, and their computational complexity does not depend on the number of aircraft, but only on the size of the physical problem of interest. (ii) Their control theoretic structure enables the use of standard methodologies to analyze them.

This article presents the comparison between three Eulerian models of the *National Airspace System* (NAS), to assess their respective accuracy, computational efficiency, and predictive capabilities. This study is thus motivated by the need to efficiently model NAS. We are implementing the three models on a graph developed in earlier work, based on one week of ASDI/ETMS data <sup>a</sup>.

The field of Eulerian models for the NAS has been pioneered by the award winning AIAA article of Menon et al.<sup>3</sup> This article is strongly inspired by hydrodynamic theory for highway traffic flow, in particular the work of Lighthill, Whitham and Richards,<sup>4,5</sup> and its discrete counterparts in the highway traffic literature.<sup>6,7</sup> This framework is sometimes referred to as the *LWR theory*. Menon et al.<sup>3</sup> were the first to model air traffic flow using an Eulerian framework, i.e. focusing on control volumes rather than single aircraft trajectories.<sup>8–11</sup> This work was subsequently extended by the same authors. It triggered a large interest in the *Air Traffic Management* community, leading to several articles inspired by their original approach.<sup>10,12</sup> This model was later adapted to include a stochastic framework,<sup>13,14</sup> in which data aggregation procedures enable predictions of flows in the expected sense. For this study, the Menon model<sup>10</sup> is modified to fit a graph structure developed in earlier work.<sup>15</sup> The aggregate stochastic dynamic model is based on Poisson processes, and describes the evolution of the aircraft count in each Center at discrete time steps. Adjoint based techniques<sup>16</sup> were subsequently developed for a fully continuous<sup>17</sup> NAS model (i.e. using partial differential equations), which has then been further used for modeling behavior of single agents (airlines) in the NAS.<sup>18,19</sup> In order to alleviate the problems due to network splits (this problem will be explained in detail later in this article and affects all previous models), a delay system model based on network flow techniques (inspired by the work<sup>20</sup>) was finally proposed<sup>15</sup> and successfully implemented, which does not suffer such shortcomings, but unfortunately does not so far include routing control strategies.

The goal of the paper is to implement and compare the three models above on the same benchmark problem based on a traffic flow graph model constructed in earlier work. We will thus compare the modified Menon model, the more recent delay system model,<sup>15</sup> and the fully continuous PDE model.<sup>17</sup>

This paper is organized as follows. In the next section, the formulation of the three models are summarized. Section III assesses the predictive capability of each model through a careful validation. Section IV compares the prediction capability of the different models, computational time and memory requirements. Section V underscores the strength of one of the models in terms of its ease of calibration. A discussion follows that highlights the structural differences between the three models and explains why one model may outperform another. Finally conclusions are presented in Section VII.

## II. Models

### A. The modified Menon model<sup>10</sup>

This section is based on the article<sup>10</sup> by Menon et. al.. The modified Menon model is largely based on the model outlined in the article.<sup>10</sup> It has been modified to fit the structure of the graph model that will be discussed in Section II D. First, the Menon model is summarized followed by the details of the modifications.

The Menon model is an Eulerian traffic flow model in which the air traffic flow is spatially aggregated into control volumes.<sup>10</sup> It is based on the *LWR theory* where the traffic flowing into a control volume changes the density of aircraft in the control volume and, hence, changes the outflow from the control volume. The Menon model has been adapted by keeping track of the flow rates into and out of the control volumes as well as the aircraft count within each volume. The model is also able to account for ATC actions as well as handle merging and diverging air traffic flow. The model consists of two parts, the one-dimensional control volume model and the merge and diverge routing structure.

The one-dimensional control volume model takes air traffic flow as a network of inter-connected control

---

<sup>a</sup>In the final version of the article, we will use a full year of ASDI/ETMS data, available to us through CNA.

volumes where the air traffic flows through a series of control volumes. One way to think of the model is as a sequence of cells, where each cell is a control volume. The air traffic flow and aircraft counts in a network, can be described by the discrete-time difference equation,

$$x_j(i+1) = x_j(i) + \tau_j[y_{j-1}(i) - y_j(i)] \quad (1)$$

In the above equation,  $x_j(i+1)$  is the aircraft count of control volume  $j$  at time  $i+1$ . The flow into  $j$  is  $y_{j-1}(i)$  and  $y_j(i)$  is the flow out of  $j$ . The time step  $\tau_j$  is calculated by dividing the cell dimension,  $\Omega_j$ , by the aircraft speed in the cell,  $v_j$  ( $\tau_j = \Omega_j/v_j$ ). In other words,  $\tau_j$  is the time an aircraft takes to travel through the cell.

The effects of delaying aircraft due to ATC is accounted for by recirculating some of the air traffic flow in a control volume. The recirculated air traffic flow in control volume  $j$  is defined as  $u_j$ . The physical constraint on  $u_j$  is that at time  $i$  it can not be greater than the existing flow in the cell and it can not be less than 0,

$$0 \leq \tau_j u_j(i) \leq x_j(i) \quad (2)$$

Including  $u_j$  and writing down the equation for  $y_j$ , the model can be written as a linear, discrete-time dynamic system,

$$x_j(i+1) = a_j x_j(i) + \tau_j u_j(i) + \tau_j y_{j-1}(i) \quad (3)$$

$$y_j(i) = b_j x_j(i) - u_j(i) \quad (4)$$

The coefficients,  $a_j$ ,  $b_j$ , and  $\tau_j$  handle the conversion between the air traffic flow,  $y_j$ , and the aircraft count,  $x_j$ . In other words, at a given time step,  $a_j$  is the portion of aircraft remaining in the volume, and  $b_j$  is the portion of air traffic flow leaving the volume. As was noted earlier,  $\tau_j$  is the length of time needed for the aircraft to travel the length of the control volume. The coefficients are defined in terms of  $\Omega_j$ , the control volume length, and  $v_j$ , the aircraft speed.

$$a_j = (1 - v_j \tau_j / \Omega_j), \quad b_j = v_j / \Omega_j, \quad \tau_j = \Omega_j / v_j \quad (5)$$

The Menon model assumes that velocity is constant within a given control volume. This means that  $a_j$  is always zero. That is, if there is no control from  $u_j$ , then all the aircraft in the volume travel to the subsequent volume on the next time step.

Intuitively, what is happening in equations (3) and (4) is that the aircraft count in a given control volume at time  $i+1$  depends on the number of aircraft in the volume at time  $i$ , the number of aircraft that flow into the volume, the number of aircraft that are recirculated and the number of aircraft that flow out of the volume. Over multiple time steps, aircraft will move through successive cells.

In a network of inter-connected control volumes, there may be points where air traffic coming from different directions merge into a single flow. This type of situation is referred to as a merge node. Furthermore, there may be points where the air traffic in one direction diverges into multiple flows. This type of situation is referred to as a diverge node. Because the nodes do not retain any aircraft, the conservation principle implies that for merge nodes, the resulting air traffic flow is the sum of all air traffic flows into that node. For example, if the air traffic flows  $q_{k-1}$  and  $q_{k-2}$  merge into  $q_k$ ,

$$q_k = q_{k-1} + q_{k-2} \quad (6)$$

Likewise, diverge nodes can make use of the same conservation principle and the flow along a path from a diverge node is a proportion of the flow coming into the diverge node. The proportion is defined as the divergence parameter,  $\beta$ , and is the ratio of aircraft travelling out of the diverge node along a given path over the aircraft travelling into the diverge node. In the following example, the air traffic flow diverges from the  $q_k$  to  $q_{k+1}$  and  $q_{k+2}$ ,

$$q_{k+1} = \beta q_k, \quad q_{k+2} = (1 - \beta) q_k \quad (7)$$

As mentioned earlier, since the *modified Menon model* (MMM) is implemented on a graph model of traffic flow constructed in the articles<sup>15,21</sup> and discussed in Section II D, a number of modifications were made to the original Menon model described in the article.<sup>10</sup>

1. The flights in the MMM are aggregated according to the links of the graph structure defined in the article,<sup>15,21</sup> and not the graph model presented in article.<sup>10</sup> defined by the graph.<sup>15,21</sup>
2. A link's length (physical distance) is determined from flights in the data. That is, flights in the data are aggregated according to the links in the graph. A link's start and exit location is determined by those flights' link entrances and exits. The start and exit location are used in calculating the link's length.
3. MMM contains merge-diverge nodes. A merge-diverge node is one that has both merging and diverging flows at the same time.
4. A merge-diverge node can have  $n$  ( $n \geq 2$ ) outflows, whose  $\beta$  values are determined from the data, whereas in the original Menon model  $n$  is limited to two.

## B. The delay system model

This section is based on the article.<sup>22</sup> The delay system model is a new Eulerian traffic flow model developed by Robelin et al.<sup>22</sup> It is a graph-theoretic model of traffic flow. Air traffic flow on this graph is modeled as a discrete time dynamical system. Under the assumption that air traffic flow can be accurately represented by an aggregated travel time, the behavior of aircraft flows on a single link can be modeled by a deterministic linear model with unit time delay, defined as follows.<sup>22</sup>

$$x_i(k+1) = A_i x_i(k) + B_i^f f_i(k) + B_i^u u_i(k) \quad (8)$$

$$y(k) = C_i x_i(k) \quad (9)$$

where  $x_i(k) = [x_i^{m_i}(k), \dots, x_i^1(k)]^T$  is the state vector, whose elements represent the corresponding aircraft counts in each cell of link  $i$  at time step  $k$ , and  $m_i$  is the number of cells in the link. The [forcing] input,  $f_i(k)$ , is a scalar which denotes the entry count onto link  $i$  during a unit time interval from  $k$  to  $k+1$ , and the [control] input,  $u_i(k)$  is an  $m_i \times 1$  vector, representing holding pattern control. The output,  $y(k)$ , is the aircraft count in a user-specified set of cells at time step  $k$ . The nonzero elements of the  $m_i \times 1$  vector  $C_i$  correspond to the cells in the user-specified set, and are equal to one.  $A_i$  is an  $m_i \times m_i$  nilpotent matrix with 1's on its super-diagonal.  $B_i^f = [0, \dots, 0, 1]^T$  is the forcing vector with  $m_i$  elements, and  $B_i^u$  is the  $m_i \times m_i$  holding pattern matrix, in which all nonzero elements are 1 on the diagonal and  $-1$  on the super-diagonal. Please see article<sup>21</sup> for more details about the model.

Because there is no interconnection between different links in one sector, it is straightforward to extend this modeling technique to set up a sector level model as follows. Suppose there are  $n$  links in a sector, then the state space equations for the model at the sector level can be described as:

$$x(k+1) = Ax(k) + B^f f(k) + B^u u(k) \quad (10)$$

$$y(k) = Cx(k) \quad (11)$$

where  $x(k) = [x_n(k), \dots, x_1(k)]^T$  denotes the state, and  $f(k) = [f_n(k), \dots, f_1(k)]^T$  is the [forcing] input vector (the entry count onto the sector). The [control] input vector  $u(k) = [u_n(k), \dots, u_1(k)]^T$ .  $y(k)$  represents the aircraft count in a user-specified set of cells at time step  $k$ . The matrices  $A$ ,  $B^f$ , and  $B^u$  are block diagonal, such that  $A = \text{diag}(A_n, \dots, A_1)$ ,  $B^f = \text{diag}(B_n^f, \dots, B_1^f)$ , and  $B^u = \text{diag}(B_n^u, \dots, B_1^u)$ . The vector  $C$  is given by  $[C_n, \dots, C_1]$ . The quantities,  $x_i(k)$ ,  $f_i(k)$ ,  $u_i(k)$ ,  $A_i$ ,  $B_i^f$ ,  $B_i^u$  and  $C_i$  are all defined by Equations (8) – (9).

When a center level model is created, it is necessary to include *merge/diverge* nodes in the network.<sup>10,13,14,17</sup> This is realized by taking into account *a priori* knowledge of the destination of the aircraft. More details about the merge/diverge mechanism are provided in the article.<sup>21</sup>

## C. The PDE model

This section is based on articles.<sup>16,17</sup> We consider aircraft density in the NAS as a continuum and study the generated flow.

We divide the airspace into line elements on which we model the density of aircraft. These line elements are called paths. We represent a path as a segment  $[0, L]$  and we denote by  $u(x, t)$  the number of aircrafts between distances 0 and  $x$  at time  $t$ . In particular,  $u(0, t) = 0$  and  $u(L, t)$  is the total number of aircrafts

in the path modeled by  $[0, L]$  at time  $t$ . We make the additional assumption of a stationary velocity profile  $v(x) > 0$  which depicts the mean velocity of aircraft flow at position  $x$  and time  $t$ . Applying the conservation of mass to a control volume comprised between positions  $x$  and  $x + h$ , and letting  $h$  tend to 0, one easily finds the following relation between the spatial and temporal derivatives of  $u(x, t)$ :

$$\begin{cases} \frac{\partial u(x, t)}{\partial t} + v(x) \frac{\partial u(x, t)}{\partial x} = q(t) & (x, t) \in (0, L) \times (0, T] \\ u(x, 0) = u_0(x) & x \in [0, L] \\ u(0, t) = 0 & t \in [0, T] \end{cases}$$

where  $q(t)$  represents the inflow at the entrance of the link ( $x = 0$ ) or in terms of the density  $q(t) = \rho(0, t)v(0)$ . This is an advection equation with control velocity and source term.

It can be shown using the method of characteristics that this partial differential equation admits a unique solution. Even though this framework is a purely continuous framework, we need to discretize it for the sake of computation.

We apply the Lax-Wendroff scheme to the preceding partial differential equation. We use a discrete grid on the domain  $[0, L] \times [0, T]$ :

$$x_i = \frac{iL}{M}, \quad 0 \leq i \leq M \text{ and } t_j = \frac{jT}{N}, \quad 0 \leq j \leq N$$

The Lax-Wendroff numerical scheme is based on the second order Taylor series expansion of  $u(x, t)$

$$u(x, t_{j+1}) = u(x, t_j) + (\Delta t)u_x(x, t_j) + \frac{1}{2}(\Delta t)^2 u_{tt}(x, t_j) + \dots$$

Given that  $u(x, t)$  is a solution of the partial differential equation above, we have:  $u_t(x, t) = -v(x)u_x(x, t) + q(t)$  and  $u_{tt}(x, t) = -v(x)u_{xt}(x, t) + q'(t)$

Using the expressions of  $u_t(x, t)$  and  $u_{tt}(x, t)$  in the Taylor series expansion, and replacing the spatial derivatives by central finite difference approximations:

$$\begin{aligned} u_x(x, t) &\leftrightarrow \frac{u_{i+1}^j - u_{i-1}^j}{2\Delta x} \\ u_{xx}(x, t) &\leftrightarrow \frac{u_{i-1}^j - 2u_i^j + u_{i+1}^j}{(\Delta x)^2} \end{aligned}$$

we eventually obtain the Lax-Wendroff scheme:

$$\begin{aligned} u_i^{j+1} = u_i^j &- \frac{\Delta t}{2\Delta x} v(x_i)(u_{i+1}^j - u_{i-1}^j) + \frac{1}{2} \left( \frac{\Delta t}{\Delta x} \right)^2 v^2(x_i)(u_{i-1}^j - 2u_i^j + u_{i+1}^j) \\ &+ \frac{(\Delta t)^2}{4\Delta x} v(x_i)v'(x_i)(u_{i+1}^j - u_{i-1}^j) + \Delta t q(t_j) \end{aligned}$$

The initial condition implies:

$$u_i^0 = \frac{1}{2\Delta x} \int_{x_{i-1}}^{x_{i+1}} u_0(x) dx \text{ for } 1 \leq i \leq M, \text{ and } u_0^0 = 0$$

The boundary conditions are implemented using two ghost cells on the left and right of the spatial domain. Given that the velocity is always positive, the boundary conditions can only be prescribed on the left; we use zero order extrapolation for the right boundary condition:

$$u_{-1}^j = u_0^j = 0 \text{ and } u_{M+1}^j = u_M^j \text{ for } 1 \leq j \leq N$$

Finally, when choosing the space and time steps, the CFL (Courant-Friedrichs-Lewy) condition has to be verified:

$$\left| \frac{v(x)\Delta t}{\Delta x} \right| \leq 1 \text{ for } x \in [0, L]$$

## D. Benchmark example for comparison of the three models

For the comparison, the three models described above are implemented on the same aggregate traffic flow graph model. The construction of the graph is outlined in the articles.<sup>21,22</sup> The airspace of interest for this study is depicted in Figure 1, and consists of 23 sectors of the Oakland, Los Angeles, Seattle and Salt Lake City Centers. The graph identification procedure relies on the notion of *path*, illustrated in Figure 1. We use one week of ASDI/ETMS data for this identification<sup>b</sup>, which results in the graph shown in Figure 2. For the modified Menon model, we will use  $\beta$  splits at the nodes where traffic is diverging, following the procedure outlined in Section II A. For the two other models, we will use the notion of paths, linking any origin to any destination in the graph. This idea was suggested to us by Dr. George Meyer, and is sometimes referred to as the *colored flow paradigm*. This enables us to avoid the identification of the  $\beta$  split parameters, and the resulting inaccuracies of this model. A drawback of this method is that it does not (so far) enable the use of rerouting strategies in case a user would like to implement control schemes in these model. Using the terminology in Figure 1, the graph used for this study has 217 paths, 102 links, 4069 cells (modified Menon model), 10293 cells (delay model), and 43400 gridpoints (PDE model). It consists of 10 high altitude sectors, includes three major airports (SFO, SJC and OAK). The number of flights used for this study for a single day is on the order of 8000.

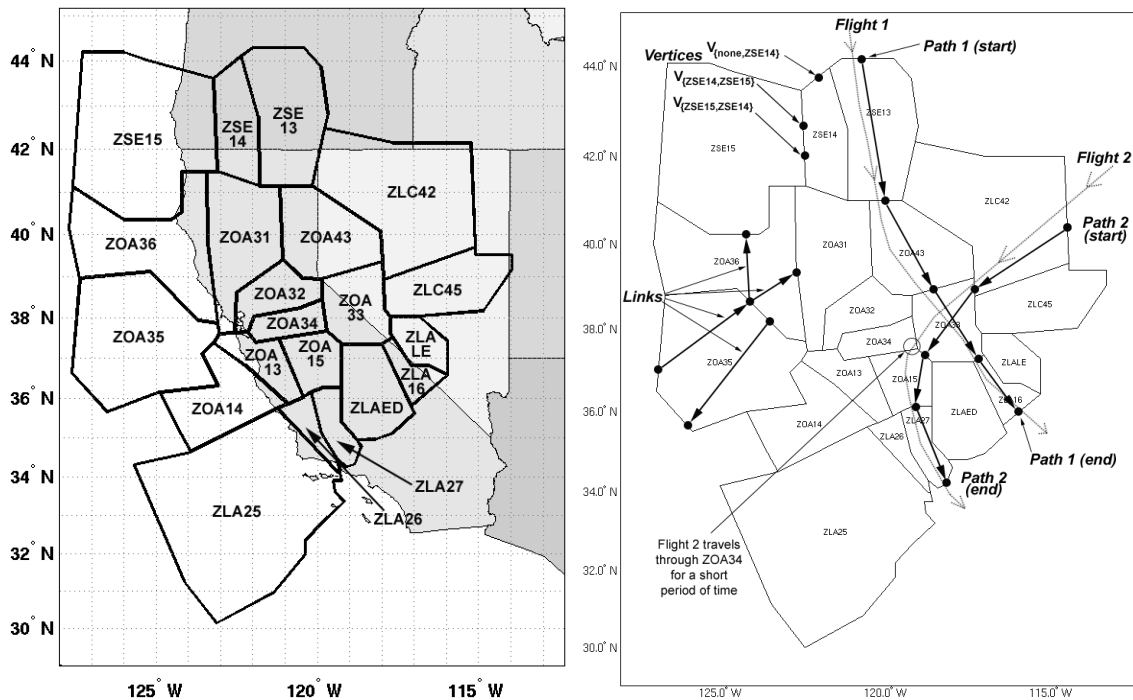


Figure 1. Left: Map of the region of the airspace considered in this study: the Oakland ARTCC, called ZOA, a portion of Los Angeles ARTCC, called ZLA, a portion of Salt Lake City ARTCC, called ZLC, and a portion of Seattle ARTCC, called ZSE. Right: Examples of vertices and links; trajectories and paths.

The parameter identification used for the modified Menon model is straightforward: following<sup>12</sup> we average all velocities of all aircraft over one week for the airspace of interest. For the delay model and the PDE model, we do it path by path. An example of velocity fit for one path is shown in Figure 3. The  $\beta$  split coefficients used for the modified Menon model are computed by dividing the number of aircraft on a branch from a split by the total number of aircraft exiting the split. The cell dimension in the modified Menon model is calculated as the distance traveled by an aircraft in one minute (our time step in the simulation). Since the average velocity is 380 knots, this gives the cell dimension to be 11 km. For the delay system model, the cell dimension is time-based and is one minute in length.

The inflow conditions for the three models is extracted from the ASDI/ETMS data for one day. Each flight in the data is analyzed in terms of its time of arrival in one of the sectors under consideration. Additionally, the delay system model and the PDE model also analyze a flight's path according to the details in.<sup>21,22</sup>

<sup>b</sup>In the final version of the article, we will use a full year of ASDI/ETMS data, available to us through CNA.

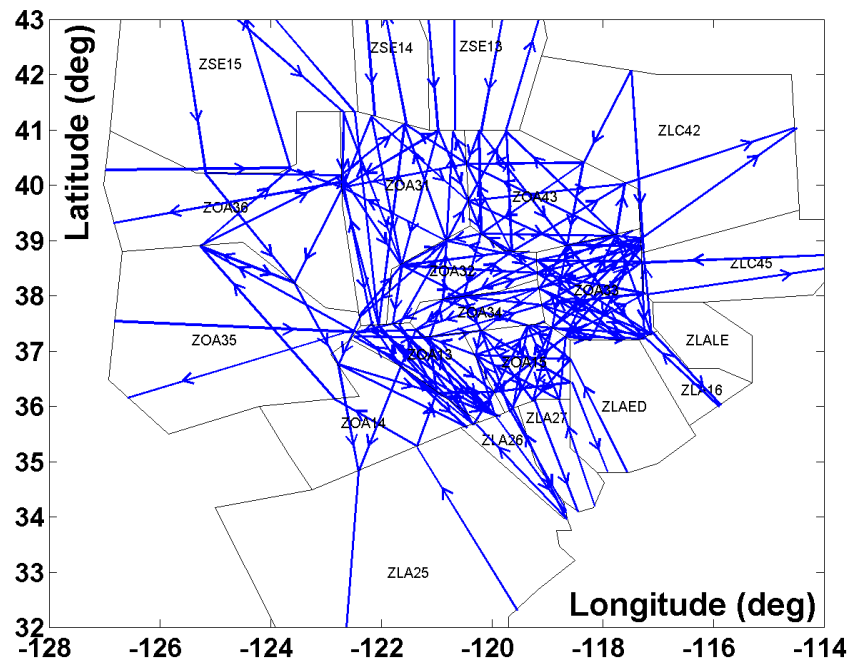
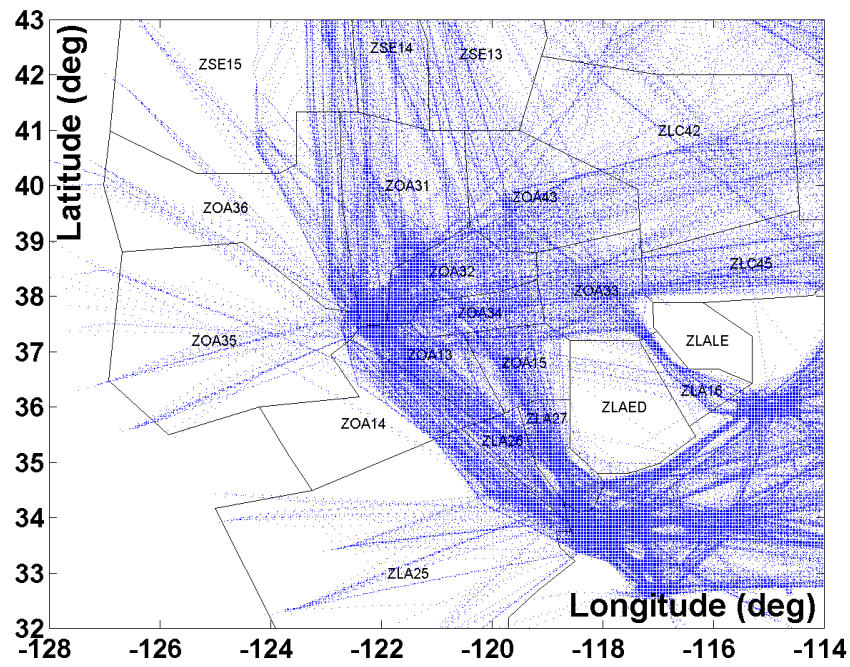


Figure 2. Top: *Flight tracks in Oakland Center and nearby airspace, for one week (5 gigabytes) of ASDI/ETMS data.* Bottom: *Graph model representing the flow patterns on the left, composed of 312 links.*

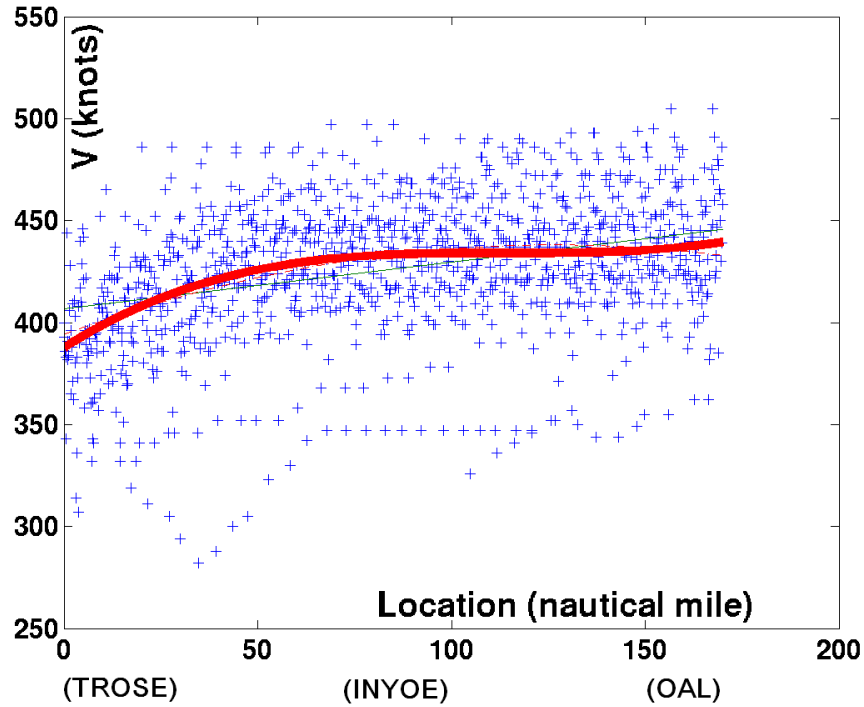


Figure 3. A typical velocity profile along a path.  $x$ -axis: positions from the starting point of a path in the model;  $y$ -axis: velocities in knots. A third order curve is used to fit the velocity profile. Typically, flights going through this path (passing through way-points TROSE-INYOE-OAL) pop-up from low altitude airspace and climb up to high altitudes.

### III. Model validation

The models are validated against ASDI/ETMS data and their respective performance are compared. Simulations are performed from 8:00am GMT on January 24th, 2005 to 8:00am GMT on January 25th. The input to the models is the number of aircraft entering the considered region (Oakland Center). The predicted states are computed from each model and compared with the actual data.

Sector counts predicted by the ATC models are first compared with the real air traffic data. Our study shows that all the sector counts predicted by the three models and ASDI data differ by noise of a non-negligible magnitude, because 1) for the delay system model, the travel time on a link in the network is computed as the average travel time for all flights in the data set used for the identification; 2) for the PDE model, the velocity profile of each path is filtered from sampled velocities and only several modes are preserved; 3) for the modified Menon model, the split ratios are computed from historical data which usually do not match the instantaneous ratios for a specific day and also assumes a uniform velocity across the whole network.

Fast fourier transform (FFT) is used to filter the sector counts for both the actual data and the models' data. Despite the fact that the filtered sector counts, produced by a FFT, may be less than zero, when we apply the inverse FFT or produce the final count results, we ensure that the counts are positive. Applying a FFT to the data requires the appropriate number of modes. To determine a proper mode a small experiment involving cumulated error is performed. Based on the noise level and the variance in the data, reproducing high frequencies does not make sense for the problem of interest. The cumulated count error is the aggregated error calculated as the absolute difference between the model's sector count and the actual sector count, over the course of a simulation. Figure 1 shows how the cumulated error increases as the number of modes increases. Note that the total error levels off when the number of modes is around 20. For this reason, 20 is chosen as the FFT mode to filter the data. Choosing a number of modes less than 20 would lead to unrealistic filtered data (as can be checked very easily in practice).

Figure 4 shows the predicted and actual sector counts as a function of time in three sectors (ZOA32,

Number of modes	3	5	10	20	40	50
Delay system model (thousands)	3.2	3.5	3.9	4.0	4.1	4.2
PDE model (thousands)	2.8	2.9	3.0	3.2	3.3	3.4
Modified Menon model (thousands)	0.8	0.8	1.2	1.3	1.4	1.3

**Table 1.** *Cumulated error.*

ZOA33 and ZOA34). For the first four rows, the curve in each plot represents the filtered sector counts and overlays the unfiltered results. The bottom row of figures in Figure 4 show the comparison between each model and the filtered real sector counts. From the figures we can see that all the models correctly predict the trends of sector counts.

A similar comparison is done with inflows into the sectors. Inflows are the number of aircraft entering a certain sector in a unit of time (one minute in our study). Figure 5 shows the predicted inflows into three sectors (ZOA32, ZOA33 and ZOA34), as well as the real inflows into these three sectors. For ZOA32, the inflows count the number of aircraft arrivals from sectors ZOA31, ZOA43, ZOA33, ZOA34, ZOA13, as well as flights originating in ZOA32. For ZOA33, the inflows count the number of aircraft arrivals from sectors ZOA15, ZOA34, ZOA32, ZOA43, ZLC42, ZLC45, ZLAL, ZLA16, ZLAED, as well as flights originating in ZOA33. For ZOA34, the inflows count the number of aircraft arrivals from sectors ZOA13, ZOA15, ZOA33, ZOA32, as well as flights originating in ZOA34. Please refer to Figure 1. The curve in each plot represents the filtered inflows. The bottom row of figures in Figure 5 show the comparison between the filtered inflows of each model and the filtered real inflows. From the figures we can see that all the models correctly predict the trends of the inflows into sectors.

## IV. Comparison

From Figures 4 and 5, the modified Menon model displays the best prediction capabilities among all the models. As can be seen in the last rows of Figures 4 and 5, the sector count and inflow predictions of the modified Menon model are closer to the real situation, compared with the other two. In comparing the three models we will quantify each model's error as well as their computational efficiency.

### A. Error analysis

The error analysis involves three comparisons: cumulated occurrence of sector count error breach ( $S$ ), the cumulated sector count error and the instantaneous sector count error. Following the article,<sup>22</sup>  $S$  is defined as the summation of time intervals under the condition that difference of sector counts between the simulation and real data is greater than or equal to a user-specified capacity limitation, within a certain time window. This is summarized in Equation (12).

$$S = \sum_{k=1}^T \mathbb{I}_{\{|y_{\text{sim}}^{(k)} - y_{\text{real}}^{(k)}| \geq C_s\}} \quad (12)$$

where  $\mathbb{I}$  represents the indicator function. The sector count is denoted by  $y(k)$  (real and simulated), and  $C_s$  is a user-defined capacity limitation. The time window we choose in our simulation is 1440 minutes (24 hours), i.e.  $T = 1440$ . To measure the similarity in the simulation and the real data, different values of  $C_s$  are utilized, and plots of number of breaches versus  $C_s$  are shown in Figure 6. As the value of  $C_s$  increases, the breach length for each model tends to zero. This is because  $C_s$  is the aircraft count error limit. For sectors ZOA32 and ZOA33, the delay system model and the PDE model are close to zero breach length when the aircraft count error limit is about 10 aircraft. The modified Menon model, on the other hand, is close to zero breach length when the aircraft count error limit is five. For Sector ZOA34, the PDE model and the modified Menon model have similar breach lengths which are close to zero around five aircraft. The delay system model, on the other hand, does not exhibit the same behavior, and its breach length is zero only after the aircraft error limit is set to 20. The reason for this will be explained in a later section.

Because of the noise level in the data, the cumulated sector count error and the instantaneous sector count error is performed on the filtered data as well as the unfiltered data.

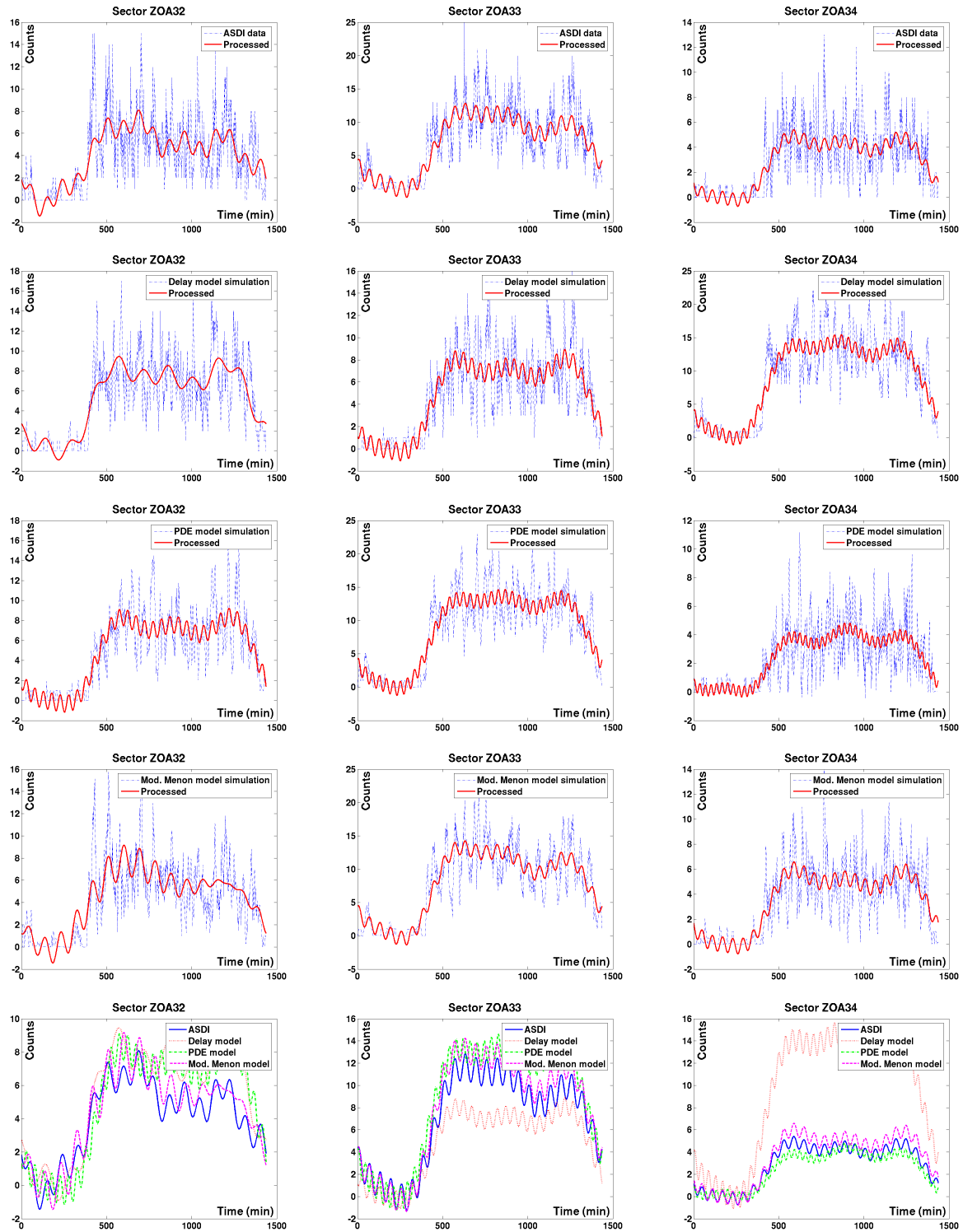


Figure 4. First row: Real aircraft sector counts. Second row: Prediction of the delay system model. Third row: Prediction of the PDE model. Fourth row: Prediction of the modified Menon model. Bottom: Comparison of the three models with the real data. Curves represent the processed sector counts when noise is filtered.

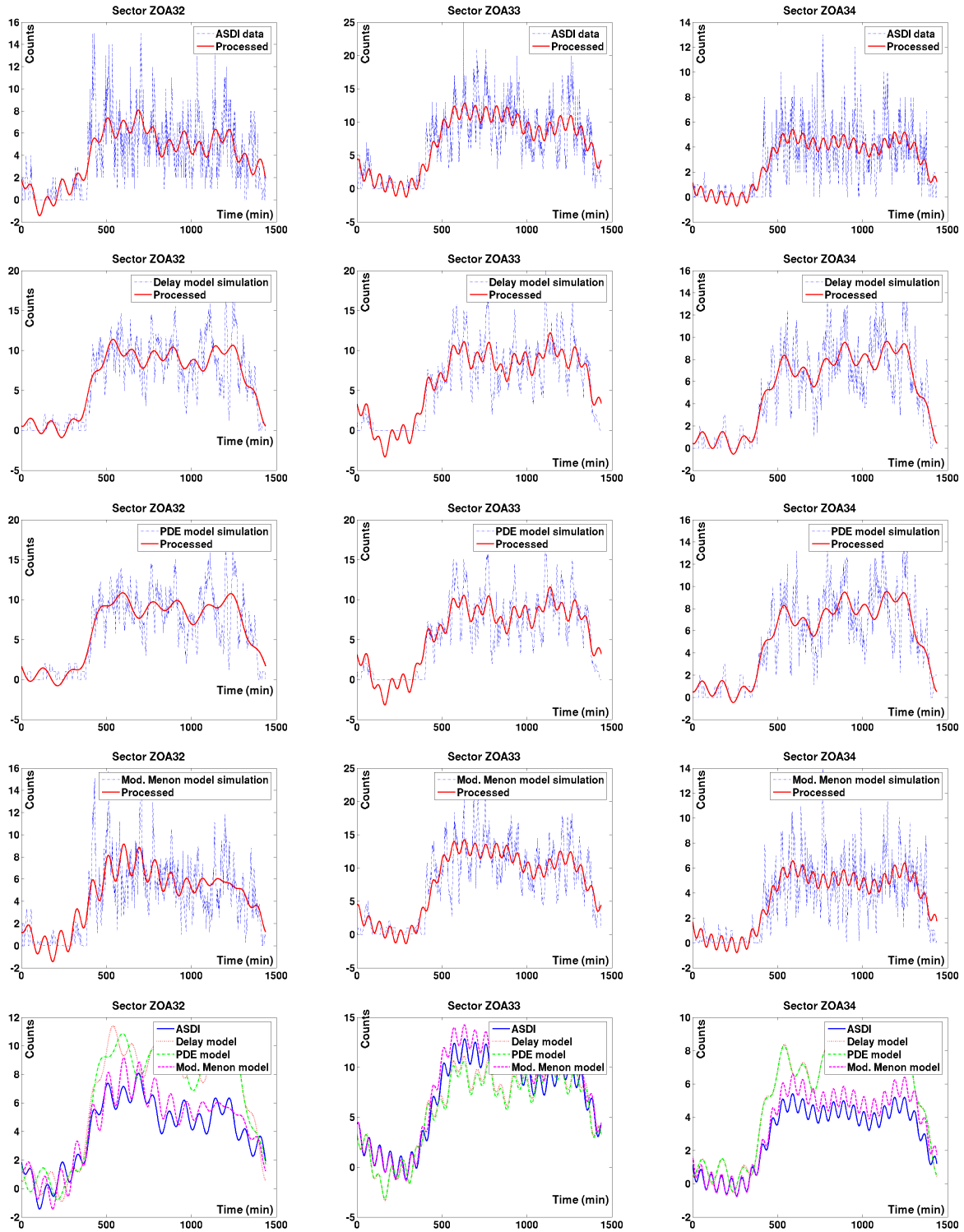


Figure 5. First row: Real inflows. Second row: Prediction of the delay system model. Third row: Prediction of the PDE model. Fourth row: Prediction of the modified Menon model. Bottom: Comparison of the three models with the real data. Curves represent the processed inflows when noise is filtered.

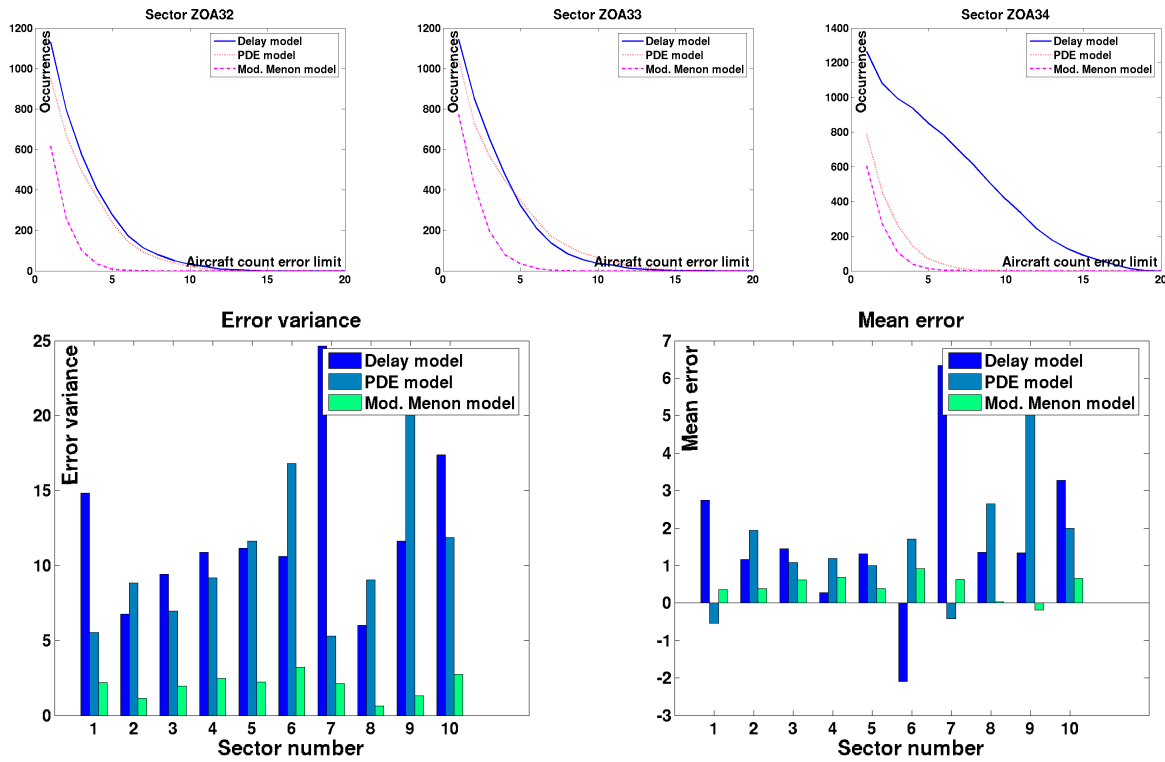


Figure 6. Top: Occurrences of breach of sector count error for three sectors in the Oakland Center. Bottom: Mean and variance of prediction errors of the three models.

The cumulated sector count error is the aggregated error calculated as the summation of the absolute difference between the model's sector count and the actual sector count, over the course of a simulation (one day) for both the filtered counts and the unfiltered counts. Figure 7 shows the cumulated error for the filtered data compared to the cumulated error for the unfiltered data. It can be seen that some of the cumulated error is due to noise. That is, the magnitude of the errors in the filtered plot are less than the errors in the unfiltered plot. Furthermore, the difference between the three models is not as large in the error for filtered data as it is in the unfiltered data. This situation is seen in sectors ZOA15 and ZOA31. However, there are still several sectors, such as sectors ZOA34 and ZOA36 where the difference between the cumulated error is significant.

The instantaneous error is the difference between the models' aircraft count and the actual aircraft count for each sector at each time step in the simulation. The instantaneous error is shown for sector ZOA33 in Figure 8. As is characteristic of the other sectors, the modified Menon model experiences less variance than both the PDE model and the delay system model. While Figure 8 shows that the PDE model overpredicts sector counts and the delay system model underpredicts sector counts, this is not necessarily the case for the other sectors.

## B. Computational efficiency

For all three models, it takes approximately ten minutes to convert the aggregate traffic flow graph model referred to in Section II D according to each model's specifications. Table 2 lists the CPU time and memory usage for the three models to predict inflows and sector counts. The analysis is done for 10 high altitude sectors in the Oakland Center, for each minute over 24 hours embedded in a set of 23 high altitude sectors, in order to eliminate undesirable boundary effects (see map in Figure 1).<sup>c</sup> The delay model has the quickest running time (six minutes), which is about 10 times faster than the PDE model and 15 times faster than the modified Menon model. The difference between the delay model and the PDE model is that the time increments required for a PDE model simulation are smaller than the delay unit used in the delay model.

<sup>c</sup>The computations are done on a 1.4 GHz CPU, 512 MB RAM PC running Linux, using c++ programming language.

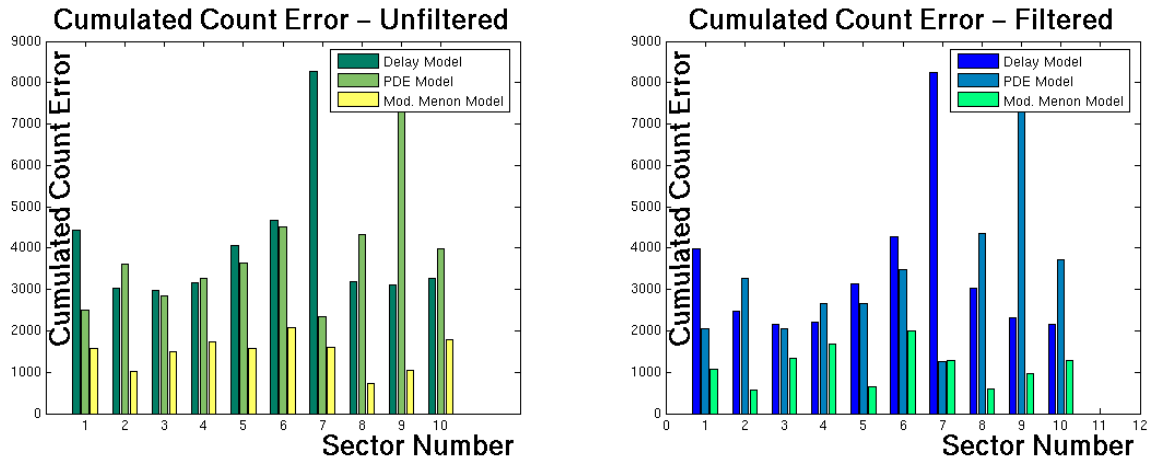


Figure 7. The cumulated sector count error for each model in each sector in the airspace. Left: The error of the unfiltered data. Right: The error of the filtered data.

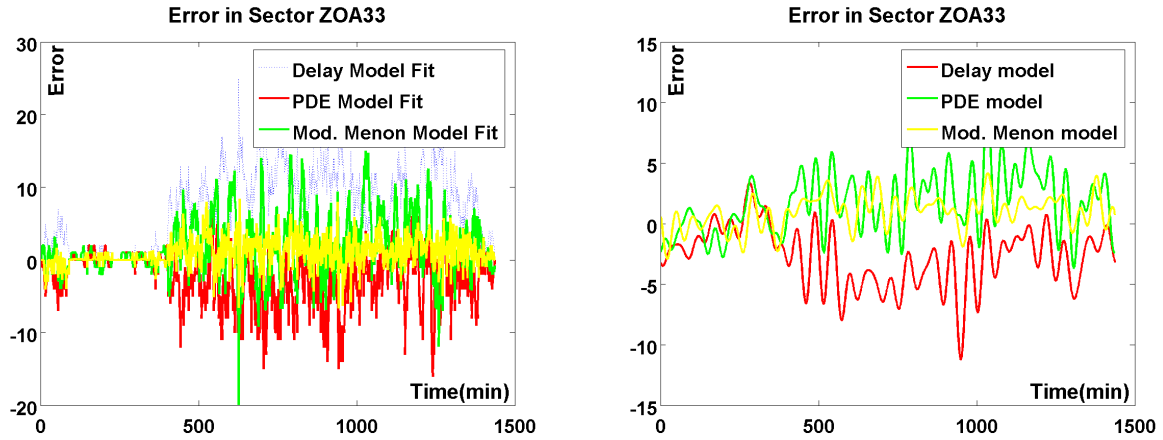


Figure 8. The instantaneous error for sector ZOA33. Left: The error of filtered data. Right: The error of unfiltered data.

The reason why the PDE model and the delay model are significantly faster than the modified Menon model is that the modified Menon model must keep track of all the merge diverge nodes in the system. In order to do this, at each time step, there are a number of matrix multiplications in that model must be computed in order to account for all merge and diverge nodes. For the PDE model and the delay model the aircraft count updates are based on only the previous counts and the path length (see Section II D).

	Delay model	PDE model	Modified Menon model
CPU time (minutes)	6	50	90
Max memory usage (MegaBytes)	395	481	376

Table 2. Computational efficiency (runs performed on a 1.4 GHz CPU, 512 MB RAM PC running Linux, using c++ programming language).

## V. An example of the calibration of the delay system model

The delay system model models the travel time along a given link as the average travel time for all flights on that link in the aggregate traffic flow graph model (see Section II D). Because link travel time is only

the average travel time, there are a number of over/under predictions that occur in the sector counts and inflows. From Sections III and IV A, the difference between the delay model's prediction and the real data can be significant. This is mainly due to insufficient samples (data set size) in the data used to build the model<sup>d</sup>. To make the model perform better, the link travel times need to be calibrated.

In the following calibration, three representative sectors are chosen for calibration: 1) sector ZOA32, in which a large percent of aircraft in this sector pop-up from low altitudes (departures flights to the East Coast); 2) sector ZOA33, which is the busiest sector in the Oakland Center with major flows and relatively few flight pop-ups or descents; 3) sector ZOA35, in which a majority of flights descend into the Bay Area TRACON.

To calibrate the delay system model, link lengths are modified to account for the difference between the predicted sector counts and real sector counts. Intuitively what is happening when a link is shortened is that the flights traveling along that link are moving at a faster velocity. Therefore the sector counts decrease. On the other hand, sector counts increase when the links in the sector are lengthened.

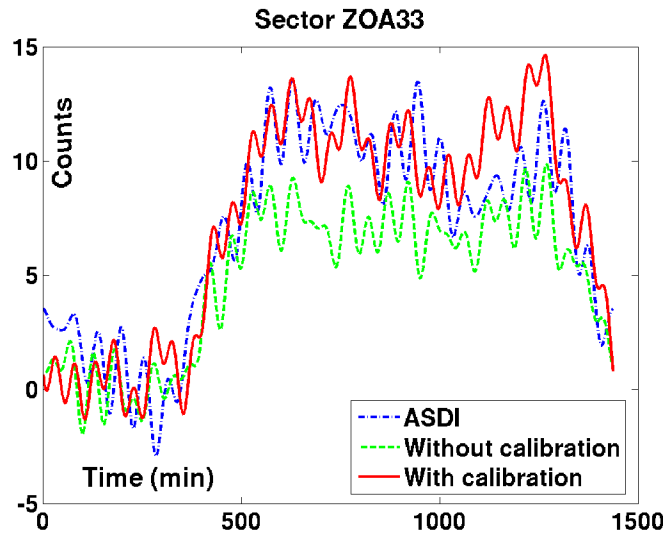


Figure 9. By lengthening certain links in sector ZOA33, the predicted sector counts are calibrated to match the the real sector counts. This modification of the link length is justified by the patterns of the flow.

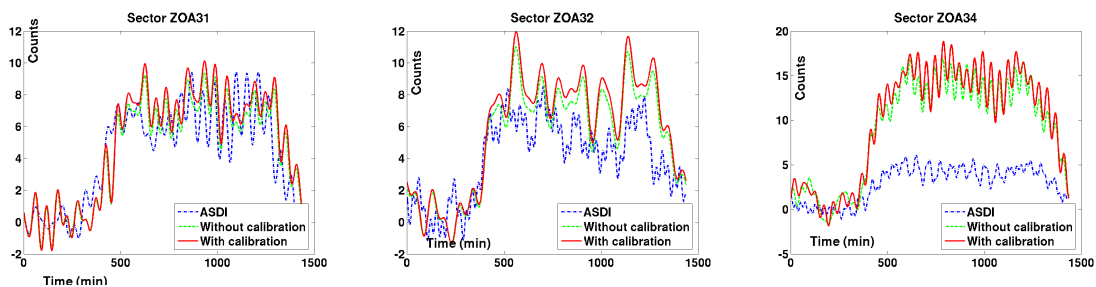


Figure 10. Lengthening certain links in sector ZOA33, the changes of the predicted sector counts in other sectors are negligible.

Figure 9 shows the calibration results when the links with most traffic are lengthened by 10% to make up for the under-predicted sector counts in sector ZOA33. At the same time, the changes of link lengths in sector ZOA33 do not affect the sector counts in other sectors, as shown Figure 10.

Figure 11 shows the histogram of traveling times<sup>e</sup> of flights going through the links that were lengthened. The calibrated link length is within the span of travel times.

<sup>d</sup>In the final version of the article, we will use a full year of ASDI/ETMS data, available to us through CNA.

<sup>e</sup>Remember that the link length in the delay system model is defined by travel time.

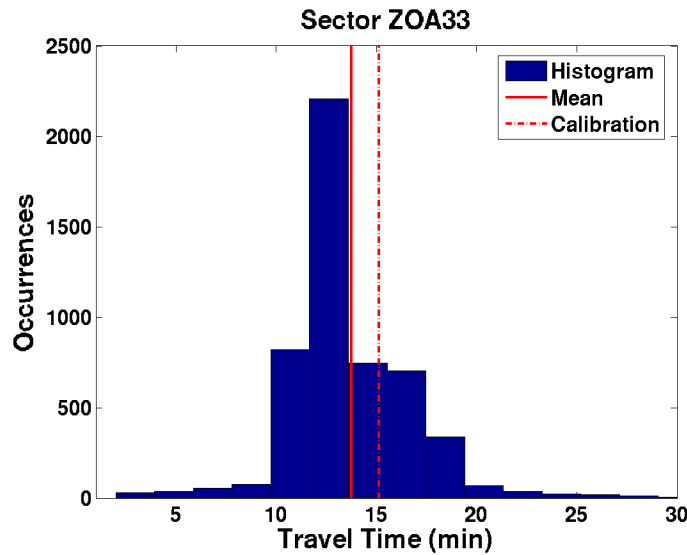


Figure 11. Histogram of the flight travel times in the links that are lengthened for the calibration of the delay system model. The calibrated link length falls in the ‘confident’ range of the travel times.

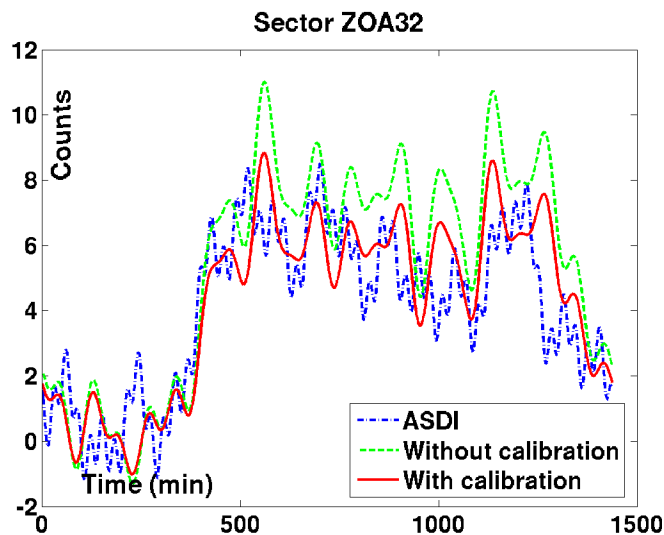


Figure 12. By shortening certain links in sector ZOA32 using features in the airspace (for example pop-ups or descents), the predicted sector counts become closer to the real sector counts. This is because the flight speed that was used in the original model (without calibration) is too slow compared to the actual flight speed. Shortening links means increase flight speed in the model so that flights stay a shorter time in the sector, therefore the sector counts decrease.

Figure 12 and 13 show the calibration results for sector ZOA32 and ZOA34, respectively. Please note that half of the flights (416 out of 839) in sector ZOA34 are descending. Decreasing the descending link lengths by 30% makes the model significantly more accurate.

Since most flights in sector ZOA34 are descending, changing the links’ lengths in sector ZOA34 does not affect the sector counts in the other sectors because these flights terminate in this sector. On the other hand, since many flights in sector ZOA32 are popping-up (360 out of 1357), changing the links’ lengths in sector ZOA32 affects counts in other sectors.

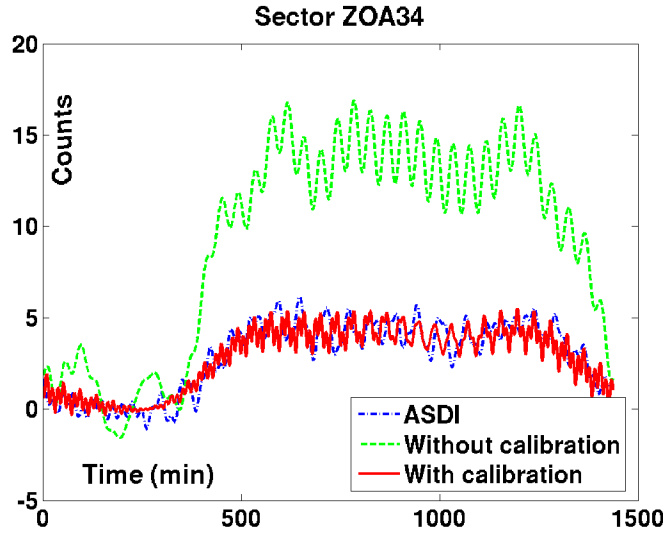


Figure 13. By shortening certain links in sector ZOA34, the predicted sector counts are closer to the real sector counts. This is because the speed of the flights that was used in the original model (without calibration) is too slow compared with the actual flight speed. Shortening links means increase flight speed in the model so that flights stay a shorter time in the sector, therefore the sector counts decrease.

## VI. Critical differences in the three models - interpretation

In Sections III and IV, one surprising result stands out: despite the drastic modeling simplifications assumed by the modified Menon model (uniform speed over the full NAS), its sector count and inflow predictions consistently outperform the other two models'. In this section, the three models are qualitatively compared in order to explain this result.

In terms of the velocity of the aircraft flow, the modified Menon model is the roughest and the PDE model is the finest. The modified Menon model uses an average velocity as the speed of all aircraft in the model. The delay system model assumes average velocities on a given *link*. So, a particular path, composed of consecutive links, has different speeds. For the PDE model, the velocity along a link is calculated using least-squares and is continuous along a path (see Section II D for more details).

In terms of the diverge nodes, the modified Menon model is also the roughest and the PDE model and delay system model are much finer. The modified Menon model calculates a fixed ratio of outgoing flow at a diverge node based on the data set. The PDE model and the delay system model generate a path through the network for each incoming flight, as outlined in article.<sup>22</sup> It is surprising that the modified Menon model, a more general and more assumptive model, exhibits fewer sector count and inflow errors than the other two models.

The critical difference between the three models is in how they handle the diverge nodes. For example, consider a hypothetical case of predicting the course of one flight arriving in sector ZOA14 and travelling through Sectors ZOA13, ZOA34, ZOA32 and ZOA43 (see Figure 1). The simulation initialization for the PDE model and the delay model consists of creating a path in the network for this flight. During simulation, the aircraft will travel through the network along the path at a velocity that has been predetermined. If the predetermined velocity is faster than the actual velocity of the flight, then at some future time, the sector count error at, say ZOA43, will be one. For the modified Menon model, no path is created and the aircraft will move through the network depending on the predetermined  $\beta$  values at the diverge nodes. It may be the case, that the sector count error in ZOA43 will only be 0.4 since the  $\beta$  value at each diverge node takes only a fraction of the aircraft flow at each diverge node. However, there will be other sector count errors that will sum up to one (since the aircraft is conserved). In other words, the sector count error of the PDE model and delay model is concentrated in one sector. The modified Menon model, on the other hand, distributes the sector count error across a number of sectors.

Since the PDE model and the delay model know beforehand the path of an aircraft, the velocity along

the links is critical. If the velocity along the link is incorrect, then the simulation will either be ahead or behind the actual flights. Section V discussed the ease at which the delay model can be calibrated to fit the flight data. In particular, Figure 13 proves that the delay model will accurately predict the sector counts if the velocities are correct. Similar results can be shown for the PDE model.

## VII. Conclusion

Three Eulerian models are implemented on an existing graph model of air traffic flow achieved in earlier work and are applied to high altitude traffic for a full Air Traffic Control Center of the National Airspace System. Each model is implemented on the same aggregate traffic flow graph model and simulated over an entire day. Compared to flight data, the models show good predictive capabilities. The models are also compared to each other in terms of their predictive ability, computation time and memory requirements. An example of calibration of one of the models to fit the real flight data better is shown.

Future work will be to use a full year of ASDI/ETMS data to construct the graph model and to study hourly/weekly patterns of air traffic flows to show how using these patterns can improve the respective predictive capabilities of each of the models. More simulations, including different days and controlled experiments, will be run in order to underline the strengths and weaknesses of each model.

## Acknowledgments

This work was supported by NASA under Task Order TO.048.0.BS.AF. We are thankful to Dr. Shon Grabbe for his help with ASDI/ETMS data and FACET. We are grateful to Dr. Gano Chatterji for his suggestions regarding the models of the National Airspace System. We want to acknowledge Dr. George Meyer for fruitful conversations on air traffic control and his ongoing support for our research, and to Charles-Antoine Robelin for his help with generating the initial model, sharing his source code and helping with the graphs presented in this article. We are grateful to Larry Hogle for helping with the collaboration between UC Berkeley and NASA Ames through the UARC.

## References

- <sup>1</sup>NOLAN, M. S., *Fundamentals of Air Traffic Control*, Brooks Cole, 4th ed.
- <sup>2</sup>DEVASIA, S., HEYMANN, M., and MEYER, G., "Automation Procedures for Air Traffic Management: A Token-Based Approach," *Proceedings of the American Control Conference*, Anchorage, AK, May 2002, pp. 736–741.
- <sup>3</sup>MENON, P. K., SWERIDUK, G. D., and BILIMORIA, K., "A new approach for modeling, analysis and control of air traffic flow," *AIAA Conference on Guidance, Navigation, and Control*, Monterey, CA, August 2002, AIAA Paper 2002–5012.
- <sup>4</sup>LIGHTHILL, M. J. and WHITHAM, G. B., "On kinematic waves. II. A Theory of traffic flow on long crowded roads," *Proceedings of the Royal Society of London*, Vol. 229, No. 1178, 1956, pp. 317–345.
- <sup>5</sup>RICHARDS, P. I., "Shock waves on the highway," *Operations Research*, Vol. 4, No. 1, 1956, pp. 42–51.
- <sup>6</sup>DAGANZO, C., "The cell transmission model: a dynamic representation of highway traffic consistent with the hydrodynamic theory," *Transportation Research*, Vol. 28B, No. 4, 1994, pp. 269–287.
- <sup>7</sup>DAGANZO, C., "The cell transmission model, part II: network traffic," *Transportation Research*, Vol. 29B, No. 2, 1995, pp. 79–93.
- <sup>8</sup>MENON, P. K., SWERIDUK, G. D., LAM, T., and CHENG, V. H. L., "Air traffic flow modeling, analysis and control," *AIAA Conference on Guidance, Navigation, and Control Conference and Exhibit*, Austin, TX, August 2003, AIAA Paper 2003–5712.
- <sup>9</sup>MENON, P. K., SWERIDUK, G. D., LAM, T., DIAZ, G. M., and BILIMORIA, K. D., "Computer-aided Eulerian air traffic flow modeling and predictive control," *AIAA Conference on Guidance, Navigation, and Control*, Providence, RI, August 2004, AIAA Paper 2004–2683.
- <sup>10</sup>MENON, P. K., SWERIDUK, G. D., and BILIMORIA, K., "New approach for modeling, analysis and control of air traffic flow," *AIAA Journal of Guidance, Control and Dynamics*, Vol. 27, No. 5, 2004, pp. 737–744.
- <sup>11</sup>SRIDHAR, B. and MENON, P. K., "Comparison of linear dynamic models for air traffic flow management," *16<sup>th</sup> IFAC world congress*, Prague, Czech, July 2005.
- <sup>12</sup>MENON, P. K., SWERIDUK, G. D., and BILIMORIA, K., "New approach for modeling, analysis and control of air traffic flow," *AIAA Journal of Guidance, Control and Dynamics*, Vol. 27, No. 5, 2004, pp. 737–744.
- <sup>13</sup>ROY, S., SRIDHAR, B., and VERGHESE, G. C., "An Aggregate Dynamic Stochastic Model for Air Traffic Control," *Proceedings of the 5<sup>th</sup> USA/Europe ATM 2003 R&D Seminar*, Budapest, Hungary, June 2003.
- <sup>14</sup>SRIDHAR, B., SONI, T., SHETH, K., and CHATTERJI, G., "An Aggregate Flow Model for Air Traffic Management," *AIAA Conference on Guidance, Navigation, and Control*, Providence, RI, August 2004, AIAA Paper 2004–5316.
- <sup>15</sup>ROBELIN, C., SUN, D., WU, G., and BAYEN, A. M., "En-Route Air Traffic Modeling and Strategic Flow Management using Mixed Integer Linear Programming," *INFORMS Annual Meeting 2005*, New Orleans / San Francisco, Nov. 2006, Note: also submitted to the 2006 American Control Conference.

<sup>16</sup>BAYEN, A. M., RAFFARD, R. L., and TOMLIN, C. J., “Adjoint-based constrained control of Eulerian transportation networks: application to Air Traffic Control,” *Proceedings of the American Control Conference*, Boston, June 2004, pp. 5539–5545.

<sup>17</sup>BAYEN, A. M., RAFFARD, R. L., and TOMLIN, C. J., “Eulerian network model of air traffic flow in congested areas,” *Proceedings of the American Control Conference*, Boston, June 2004, pp. 5520–5526.

<sup>18</sup>RAFFARD, R., WASLANDER, S. L., BAYEN, A. M., and TOMLIN, C. J., “A Cooperative, Distributed Approach to Multi-Agent Eulerian Network Control: Application to Air Traffic Management,” *Proceedings of the AIAA Guidance, Navigation and Control Conference and Exhibit*, San Francisco, CA, Aug 2005, AIAA Paper 2005-6050.

<sup>19</sup>RAFFARD, R., WASLANDER, S. L., BAYEN, A. M., and TOMLIN, C. J., “Toward Efficient and Equitable Distributed Air Traffic Flow Control,” Submitted to *American Control Conference*, 2006.

<sup>20</sup>IAMRATANAKUL, D., MEYER, G., CHATTERJI, G., and DEVASIA, S., “Quantification of Airspace Sector Capacity using Decentralized Conflict,” *Proceedings of the 43<sup>rd</sup> IEEE Conference on Decision and Control*, Atlantis, Paradise Island, Bahamas, December 2004, pp. 2003–2009.

<sup>21</sup>ROBELIN, C. A., SUN, D., WU, G., and BAYEN, A. M., “Strategic Traffic Flow Models based on Data-Mining and System-Identification Techniques,” NASA Technical Memorandum, in preparation, 2006.

<sup>22</sup>ROBELIN, C., SUN, D., WU, G., and BAYEN, A. M., “MILP control of aggregate Eulerian network airspace models,” Submitted to *American Control Conference*, 2006.